

RESEARCH

Open Access



Experimental, Numerical, and Analytical Investigation of the Reinforced Concrete Hidden and Wide Beams

Ahmed A. Mahmoud^{1*} , Belal K. El Gani¹ , Tarek S. Mustafa¹ and Ahmed N. M. Khater¹

Abstract

This research presents an experimental, analytical, and numerical study to predict the flexural behavior of reinforced concrete hidden and wide beams embedded in slabs. The experimentally studied parameters of testing eight specimens include beam depth, beam width, and beam eccentricity from the column. The obtained test results were compared to the predictions of finite element analysis using the ANSYS program. A numerical parametric study was conducted by the ANSYS program to explore other parameters affecting the ultimate flexural strength of beams. The studied parameters encompass concrete compressive strength, steel reinforcement strength, bottom reinforcement ratio, top-to-bottom reinforcement ratio, and web reinforcement ratio. The results revealed that an increase in beam depth led to higher ultimate load and secant stiffness, along with a decrease in deflection. The increase in beam width significantly affected beam depth, resulting in increased ultimate load and secant stiffness and a slight decrease in deflection. The increase in beam eccentricity from the column resulted in a decrease in ultimate load and secant stiffness while increasing the deflection. Comparisons between experimental and numerical results were made against calculations based on the ECP 203-2017 and ACI 318-19 codes, and the comparison yielded satisfactory results.

Keywords Hidden and wide beams, Flexural behavior, Experimental study, Analytical study, Numerical analysis, ANSYS program

1 Introduction

Hidden beams are beams that have a depth that is equal to or slightly higher than the slab depth. Wide beams are beams with a width that is wider than the column width, or when the beam width is more than twice the beam's depth. Reinforced concrete hidden and wide beams have been used in construction buildings because they provide many advantages, including reducing the reinforcement congestion, reducing the quantity of the

required formwork, providing simplicity for replication, and decreasing the story height. The flexural behavior of reinforced concrete hidden and wide beams depends on beam depth, beam width, beam main reinforcement ratio, and beam eccentricity. Many researchers have studied the shear behavior of hidden and wide beams. Few researchers have studied the flexural behavior of reinforced concrete hidden and wide beams embedded in slabs.

Ozbek et al. (2019) compared projected beam behavior with the corresponding hidden beams. The results illustrated that hidden beams were able to achieve the reference strengths of projected beams after excessive up to eight times greater deformations. El Bannani (2013) showed that wide beams without web reinforcement have no size effect compared to wide beam widths.

Journal information: ISSN 1976-0485 / eISSN 2234-1315.

*Correspondence:

Ahmed A. Mahmoud

ahmed.ahmed@feng.bu.edu.eg; ahmed.m5882@gmail.com

¹ Faculty of Engineering at Shoubra, Civil Engineering Department, Benha University, 108 Shoubra Street, Shoubra 11691, Cairo, Egypt



© The Author(s) 2024. **Open Access** This article is licensed under a Creative Commons Attribution 4.0 International License, which permits use, sharing, adaptation, distribution and reproduction in any medium or format, as long as you give appropriate credit to the original author(s) and the source, provide a link to the Creative Commons licence, and indicate if changes were made. The images or other third party material in this article are included in the article's Creative Commons licence, unless indicated otherwise in a credit line to the material. If material is not included in the article's Creative Commons licence and your intended use is not permitted by statutory regulation or exceeds the permitted use, you will need to obtain permission directly from the copyright holder. To view a copy of this licence, visit <http://creativecommons.org/licenses/by/4.0/>.

Helou and Diab (2014) studied the structural system's influence on hidden beams. The results showed that the hidden beam behaves more like a slab than a beam, even under static loadings. Nadagouda and Ravi (2017) studied RC slabs with projected beams and concealed beams. The results showed that the deflection of slabs with concealed beams is higher than that of slabs with projected beams, and the grade of concrete plays an important role in decreasing the deflection. Morsy et al. (2018) concluded that for beams with a depth of less than 250 mm, the welded link web reinforcement is the most proper shear reinforcement to increase the shear capacity. Helou and Awad (2014) concluded that the use of shallow beams demands focused attention, proper in-depth analysis, and meticulous detailing to avoid high reinforcement ratios at the beam end and column junctions. Alluqmani (2020) investigated that the transversal spacing of the stirrup legs of the shallow concealed RC beams influences their strength and behavior. The transversal spacing of the stirrup legs should not exceed the lesser of 0.56 of the effective depth, or 170 mm.

Conforti et al. (2013) investigated steel fibers. The steel fibers were used because, even in small amounts, they can substitute for the minimum shear reinforcement in wide-shallow beams (WSBs) and can improve the behavior of WSBs by reducing deflection. Conforti et al. (2015) reported an experimental campaign on reinforced concrete (RC) wide-shallow beams (WSBs) with or without fibers, tested under shear and flexure. The results demonstrated that shear bearing capacity and beam ductility can be considerably increased with a relatively low fiber volumetric fraction. Abbas and Hassan (2019) showed an increase in the ultimate load of the strengthened beams with inclined, vertical carbon fiber reinforced polymer (CFRP) and beam width shear reinforcement by 19.9%, 7.14%, and 39.8%, respectively, compared with the control beam. The results mean that there is a possibility of replacing the internal shear reinforcement with externally bonded CFRP. Negheimish et al. (2011) showed that applying the same amount of CFRP reinforcement in two layers compared with one layer reduces the ultimate capacity of the test beam and reduces the effectiveness of strengthening in restricting the opening of flexural cracks; however, no negative effect was observed on the flexural stiffness.

Yasouj et al. (2015) showed that independent bent-up bars increased the shear capacity and ductility of wide beams. It was revealed that, although independent horizontal bars increased the shear capacity to some extent, the beam was less ductile through failure. Khalil (2019) concluded that the beam width-to-depth (b/d) ratio has a significant influence on the modes of failure and the shear strength of reinforced concrete wide-shallow

beams. Mawlood et al. (2021) concluded that with an increasing width-to-height ratio, the shear strength of the beam decreased. Talawar and Sonawadkar (2017) concluded that concealed beam structures are better than normal beam structures during earthquakes. Olvera (2023) showed that structures with drop beams have no significant cost differences with hidden beams while achieving noticeably better structural behavior in high-risk seismic zones. Nadagouda (2017) explained that the deflection of slabs with concealed beams is greater than that of drop beams. This can be attributed to the decrease in stiffness caused by a reduction in cross-section area. Behnam (2018) illustrated that increasing the beam depth while reducing the amount of beam longitudinal reinforcement also enhances the response of the wide beam-column connections. Moawad (2021) showed that using glass fiber segments in shallow and wide beams leads to improvements in the performance of the beams in cracking, stiffness, and ultimate capacity.

Ibrahim et al. (2018) investigated the strength of bubbling broad reinforced concrete beams with various shear steel plate kinds. This research revealed that shear steel plates are a viable replacement for stirrups since they increased yield, ultimate load, and deflection (at service load) by an average of 5%, 15%, and 9% compared to utilizing bubbles. The yield deflection is enhanced by 24%, 37%, and 27% for 3, 4, and 5 mm shear steel plate thickness, respectively, compared to 10 mm stirrups. The enhancement was 8% for all specimens when utilizing the assumptions of Yousef et al. (2023) reported that web torsional reinforcement does not consider the effect on the torsional strength of ultra-high-performance fiber-reinforced concrete (UHPFRC) beams. The maximum spacing of stirrups should be taken at a minimum of twice the beam width, or 300 mm. The minimum bar diameter of the longitudinal torsional reinforcement is 12 mm, or $(1/15)$ the web reinforcement spacing. Tapan (2014) investigated the experimental evaluation of reinforced concrete wide beams. The beams were strengthened with lattice girders to determine the impact of lattice girders on load-bearing capability. This research showed that the lattice girder-reinforced and conventionally reinforced beams exhibited comparable stiffness. The lattice-girder-reinforced beams exhibited a better resisting capacity. Mohammed et al. (2023) concluded that the deflection at yield and ultimate load were increased by an average of 20% and 28% due to the use of the shear-steel plate instead of the stirrups. Lotfy et al. (2014) concluded that the shear strength increases with an increase in the web reinforcement ratio. The shear strength is inversely proportional to the shear-span-to-effective depth ratio (a/d).

Few researchers studied the flexural behavior of reinforced concrete hidden and wide beams, and the code

Table 1 The studied parameters

Specimen model	Group no	Beam depth (mm)	Beam width (mm)	Beam eccentricity (mm)	Notes
S1E	1	160	300	0	Effect of beam depth
S2E	1	180	300	0	Control specimen of Group 1
S3E	1	200	300	0	Effect of beam depth
S4E	1	180	400	0	Effect of beam width
S5E	1	180	500	0	Effect of beam width
S6E	2	180	300	0	Control specimen of Group 2
S7E	2	180	300	250	Effect of beam eccentricity
S8E	2	180	300	350	Effect of beam eccentricity

provisions did not take into consideration the beam eccentricity from the supporting column.; therefore, this paper focused on investigating, aiming at studying experimentally the flexural behavior of eight specimens. In addition, the experimental results are examined to validate and verify the output results in the numerical models using the nonlinear finite element program ANSYS V15 (ANSYS V15, 2015). Finally, the experimental and numerical results are compared with those calculated based on the ECP 203-2019 (ECP-203, 2019) and the ACI 318-19 code (ACI Committee 319-19, 2019).

The highlights of the research are:

- Describe the experimental study conducted for eight hidden and wide RC beams subjected to two concentrated loads located at the third and two-thirds of the span at the top surface.
- Study the effect of beam depth, width, and eccentricity on the flexural behavior of hidden and wide beams embedded in slabs.
- Evaluate the failure modes, crack patterns, and load–deflection curves.
- Compare the experimental results with the numerical and analytical results.
- Suggest recommendations for designers.
- Gives recommendations that can be used in the code provisions for reinforced concrete hidden and wide beams.

2 Experimental Program

The main objective of this investigation is to conduct an experimental study on the flexural behavior of hidden and wide beams with different parameters and to understand their actual behavior. All specimens were tested as simply supported. The specimens are reinforced by main and secondary steel bars and web reinforcement. Each beam was tested under two-point top loading at the third and two-thirds of the span. The tested specimens were divided into two groups: RC-hidden and wide beams.

The experimental program aims to study the specimen's flexural response and the effects of some parameters. The studied parameters are (1) the beam depth, (2) the beam width, and (3) the beam eccentricity from the supporting column, as shown in Table 1.

2.1 Description of Tested Specimens

The test program included eight specimens, from SE1 to SE8. The beams were designed based on the Egyptian code ECP 203–2019 (ECP-203, 2019) and divided into two groups. All specimens in the first group, from SE1 to SE5, had the same total length, width, and span of 1800, 800, and 1650 mm, respectively. All specimens in the second group from SE6 to SE8 had the same total length, width, and span of 1900, 1200, and 1650 mm, respectively. Table 1 shows the dimensions and properties of the tested specimens, such as section dimensions and beam eccentricity. Figs. 1 and 2 show the structural details of the control specimen for groups 1 and 2, respectively.

2.2 Mixture Composition and Material Modeling

Table 2 shows the used concrete mix design for one cubic meter. Tests were carried out on all materials used in the experimental program to determine their mechanical properties. The used materials are cement, sand (fine aggregate), dolomite (coarse aggregate), and superplasticizer (Addicrete BVF). Five cylinders (150 mm in diameter and 300 mm in height) and three cubies (150*150*150 mm.) were cast from the batch of each specimen and tested on the specimens' testing day. The cubies were used to find the concrete cubic compressive strength (f_{cu}). Three cylinders were used to determine the concrete cylindrical compressive strength (f_c') according to ASTM C39 (ASTM International, 2015a) and were also used to draw the stress–strain curves for concrete in compression. Fig. 3 determines the strain at the maximum compressive strength and the concrete elastic modulus according to ASTM C496-96 (ASTM International, 2021). The other two cylinders were used to find the

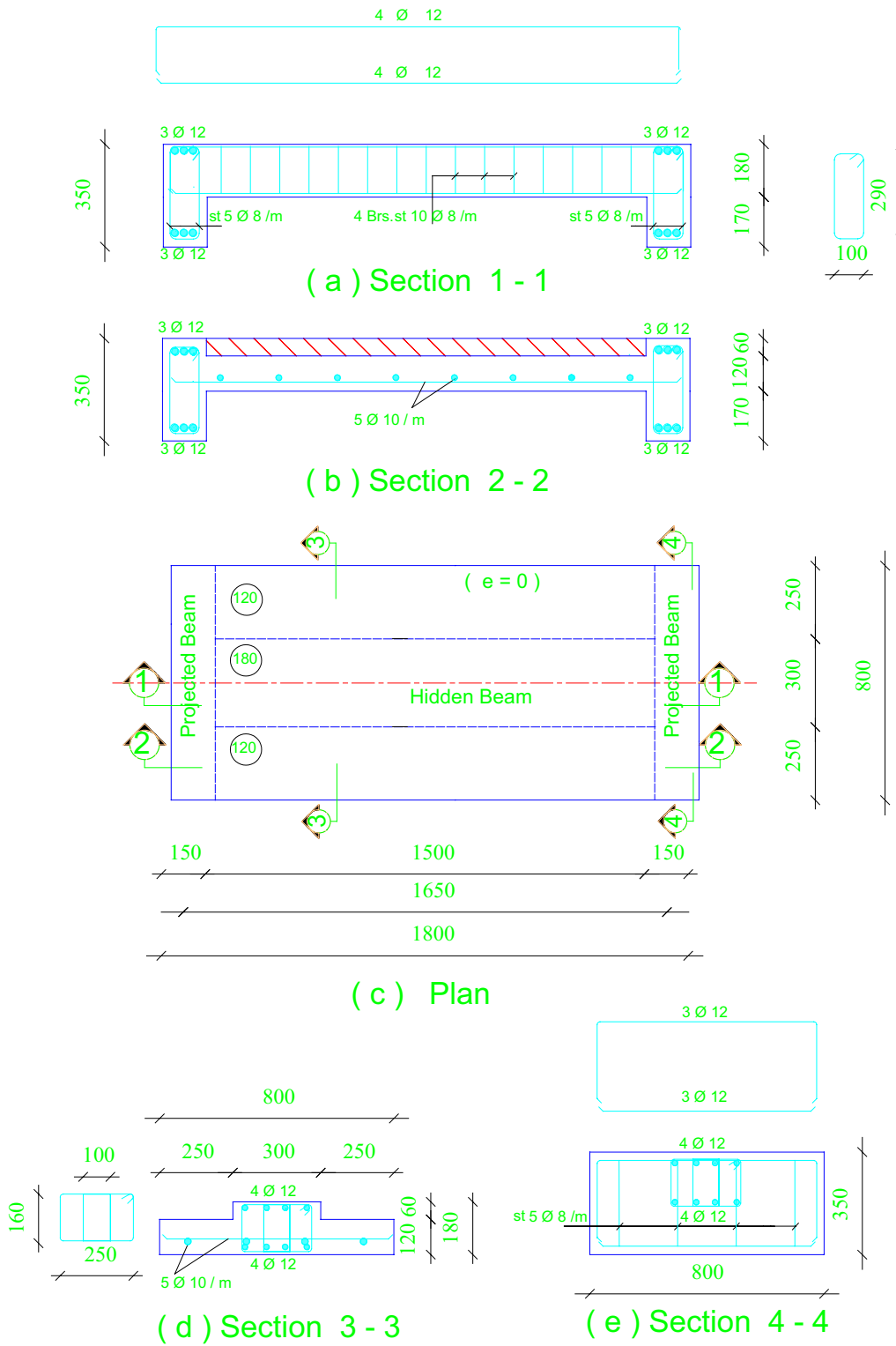


Fig. 1 Details of the tested specimen S2E (all dimensions are in mm)

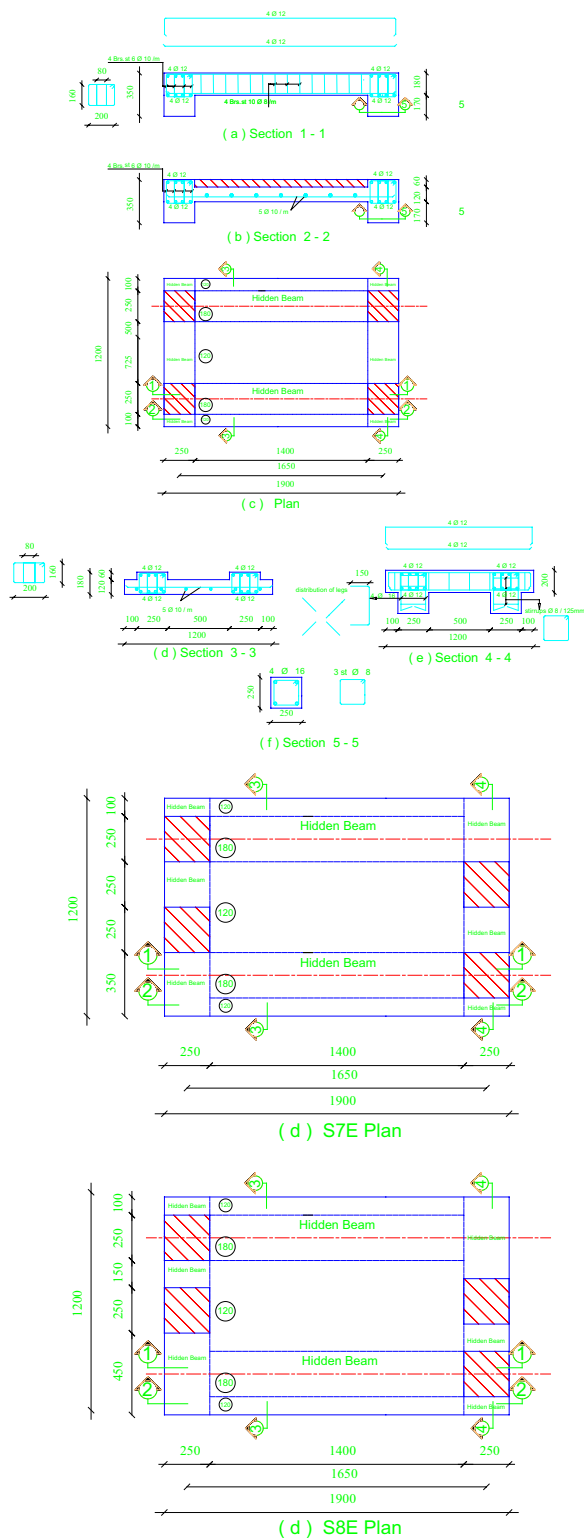


Fig. 2 a Details of the tested specimen S6E (all dimensions are in mm). b Eccentricity details of the tested specimens S7E and S8E (all dimensions are in mm)

concrete tensile strength from the splitting tensile test according to ASTM C496 (ASTM International, 2015b). Table 3 shows the mechanical properties of the used concrete. The average cubic and cylindrical concrete compressive strengths were 47 and 37.6 MPa, respectively, while the average concrete tensile strength was 3.42 MPa. The tensile strength of steel reinforcement bars was determined according to ASTM E8 (ASTM E8/ASTM E8m, 2013). The used steel reinforcement is tested at uniaxial tension. Three standard bars of 1000 mm in length from each diameter are considered to represent the yield strength of reinforcement bars. The yield strength for the steel reinforcement with diameters 8, 10, 12, and 16 mm is 337, 585, 565, and 573 MPa, respectively. The mechanical properties of the reinforcement steel are shown in Table 4. Fig. 4 shows stress–strain curves for the used steel reinforcement.

2.3 Test Setup, Instrumentation, and Test Procedure

The tests were carried out in the laboratory of the Faculty of Engineering at Mataria, Helwan University, Egypt. Figs. 5 and 6 show the test setup of groups 1 and 2, respectively, while Figs. 7 and 8 show a schematic representation of the test setup. A test machine with a capacity of 1000 kN was used. The instrumentation was used to monitor the load and the deflection. All specimens were tested as simply supported. Each beam was tested under two-point top-loading on the third and two-thirds of the span. The deflection was measured by linear variable differential transducers (LVDTs). The LVDTs were connected to beams, where two LVDTs were used at the third and two-thirds of the specimen. The laboratory's expert technicians calibrated the load cell and LVDTs before starting the test. The initial values of the devices were reset to zero through the lab program. All specimens were tested under the displacement control technique with a 1.0 mm/min rate. After each increment, measuring apparatuses were inspected, cracks were marked and demonstrated, and photos were taken. The results were recorded for the entire duration of the test, while the load was paused for manual observations and visual inspection.

3 Analysis and Discussion of the Experimental Results

The test results include (1) first crack load; (2) crack patterns; (3) failure mode; (4) failure load; and (5) load–deflection curve. The results of the eight hidden and wide beams are compared to the control specimen. The results were used to determine the effect of the studied parameters on the flexural behavior of the hidden and wide beams embedded in the slabs. Table 5 illustrates the experimental results of the eight specimens. The

Table 2 Concrete mix proportion per cubic meter

Material	Cement	Sand	Aggregate	Water	Superplasticizer	Total
Weight (kg)	450	676	1255	117	13.5	2511.5
Specific gravity (kg/m ³)	3150	2650	2650	1000	1180	2511.6
Volume (m ³)	0.143	0.255	0.473	0.117	0.012	1

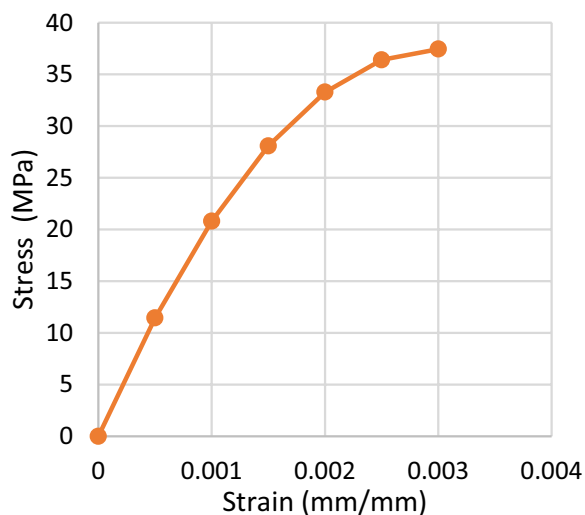


Fig. 3 Concrete stress–strain curve

collected results are (1) the first crack load due to flexure (P_{cr}); (2) the failure load (P_f) for each specimen; (3) the corresponding deflection (Δ_{cr} and Δ_f); (4) secant stiffness (S.S.); (5) displacement ductility (D.D.); and (6) toughness (T). Table 6 illustrates the comparison between specimens from Group 1 and the control specimen S2E. Table 7 illustrates the comparison between specimens from Group 2 and the control specimen S6E.

3.1 First Crack Load, Crack Patterns, and Failure Modes

This section illustrates the general behavior and crack patterns of the eight specimens. During the test and

Table 4 Mechanical properties of the reinforcement steel bars

Diameter (mm)	Area (mm ²)	Ultimate strength f_u (MPa)	Young's modulus E_s (GPa)	Poisons ratio ν
8	50.3	458	198	0.3
10	78.5	661	216	
12	113	694	217	
16	254	254	733	220

after each load interval, the load was paused to observe and mark cracks. The initial and final crack propagations were monitored by visual inspection. At the beginning of loading, a few flexural cracks formed in the regions that were exposed to pure bending.

Fig. 9 shows the crack patterns and failure modes for all the tested specimens. In the case of the control specimen S2E of group 1, at an early loading level of about 94.3 kN, fine flexural cracks formed at the mid-span. Upon increasing the load, the crack width increased to a load level of about 122.8 kN. At higher loading levels, the flexural cracks propagated along the line connecting the support and the point of load application. Finally, the beam failed by flexure at a load of 269.0 kN due to flexural cracks.

For specimens S1E and S3E, the first flexural crack is observed at the bottom at loads of 71 and 110.8 kN, respectively. Increasing the beam depth increases the first crack load P_{cr} by 25% and 17% for specimens S1E and S3E, respectively, compared to the control beam S2E. Upon increasing the load, the crack width increased at a load level of about 111.5 and 145.1 kN. At

Table 3 Mechanical properties of the concrete

Average cubic compressive strength f_{cu} (MPa)	Average cylindrical compressive strength f'_c (MPa)	Elastic modulus E_c (MPa)	Average tensile splitting strength f_t (MPa)	Poisons ratio ν	Coefficient of open shear	Coefficient of close shear
47	37.6	22,880	3.42	0.2	0.2	0.8

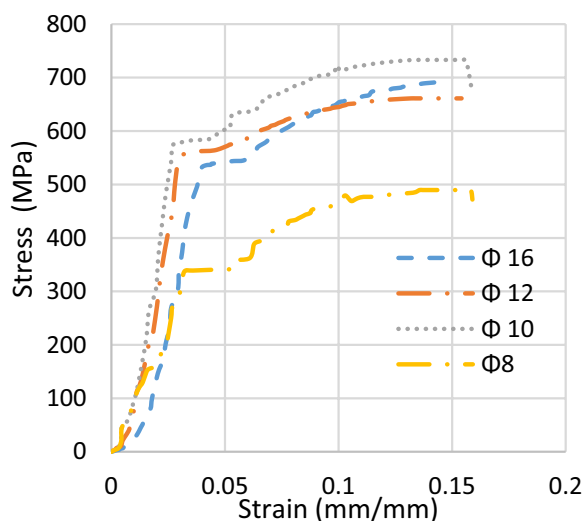


Fig. 4 Steel stress–strain curves



Fig. 5 Test setup of group 1

higher load levels, the flexural cracks propagated along the line connecting the support and the point of load application. Finally, the specimens S1E and S3E failed by flexure at a load of 251.6 and 310.3 kN, respectively.

For specimens S4E and S5E, the first flexural crack observed increases the first crack load P_{cr} by 24% and 27%, respectively, compared to the control beam S2E. Upon increasing the load, the crack width increased at a load level of about 134.2 and 210.3 kN, respectively. At higher load levels, the flexure cracks propagated along the line connecting the support and the point of load application. Finally, the beam failed in flexural at a load of 271.0 and 281.2 kN, respectively.

In the control specimen S6E of group 2, at an early loading level of about 157.1 kN, fine flexural cracks were initiated at the mid-span. Upon increasing the load, the crack width increased to a load level of about 354.3 kN. At higher load levels, the flexural cracks propagated along the line connecting the support and the point of load application. Finally, the beam failed in flexural at a load of 495.6 kN.

For specimens S7E and S8E, the first flexural crack is observed at the bottom at loads of 152 and 145.6 kN, respectively. Increasing the beam eccentricity from the column decreases the first crack load P_{cr} by 3% and 7% for specimens S7E and S8E, respectively, compared to the control beam S6E. Upon increasing the load, the crack width increased at a load level of about 305.8 and 290.60 kN. At higher load levels, the flexural cracks propagated along the line connecting the support and the point of load application. Finally, the beam failed in flexural at loads of 462.9 and 435.9 kN, respectively.



Fig. 6 Test setup of group 2

3.2 Load Deflection Curves

Fig. 10 shows the effect of beam depth on the flexural behavior of hidden and wide beams using specimens S1E, S2E, and S3E. The beam depth equals 160 mm, 180 mm, and 200 mm for specimens S1E, S2E, and S3E,

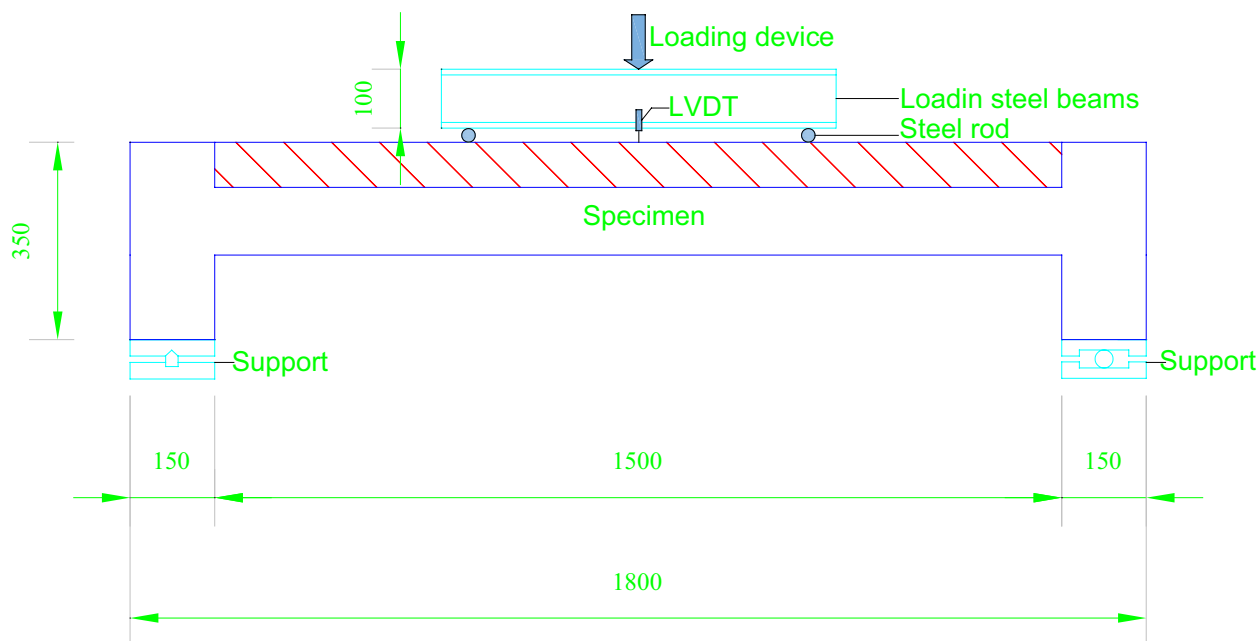


Fig. 7 Schematic test setup, instrumentation, and loading (group 1)

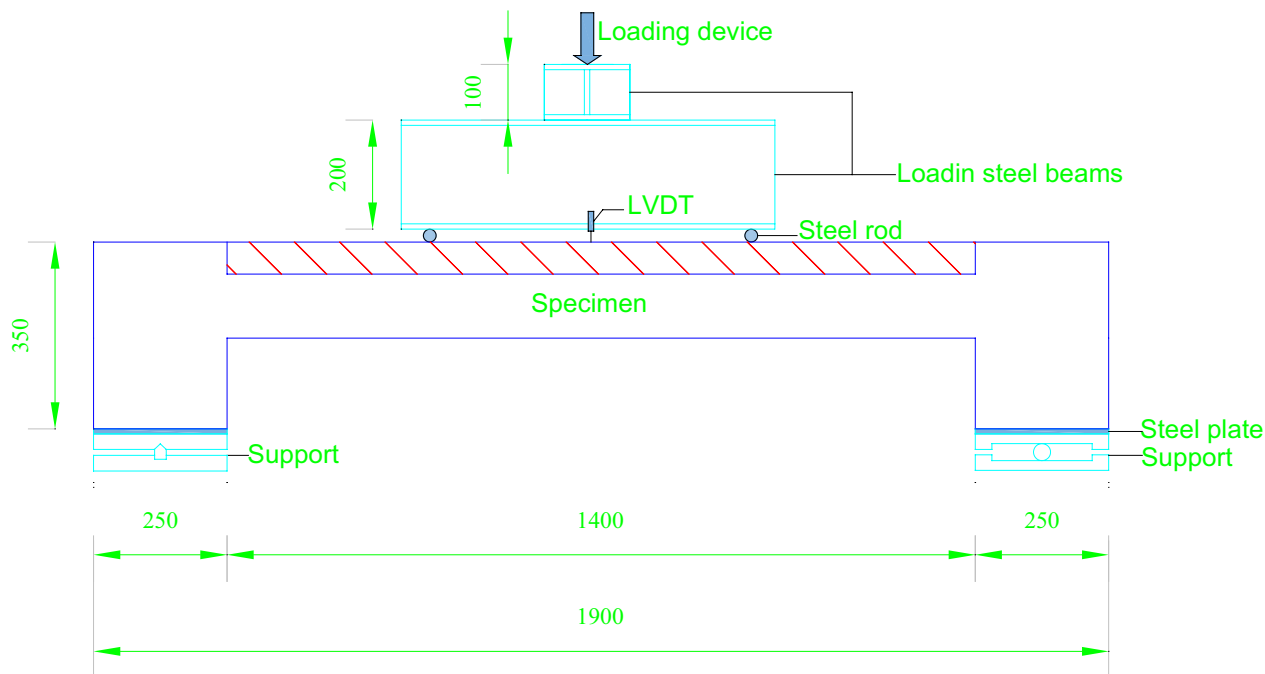


Fig. 8 Schematic test setup, instrumentation, and loading (group 2)

respectively. The results were compared with the control specimen, S2E. As shown in Table 6, the ultimate load of specimen S3E showed an increase of 15% compared to S2E. The ultimate load of specimen S1E showed a decrease of 4% compared to specimen S2E due to the

decrease in its depth. The deflection at the ultimate load of specimen S3E showed a reduction of 35% compared to the control specimen S2E. The deflection at the ultimate load of specimen S1E showed an increase of 21% compared to the control specimen S2E. The results show

Table 5 The experimental results

Specimen model	Group No	P _{cr} (kN)	Δ _{cr} (mm)	P _f (kN)	Δ _f (mm)	S.S. (kN/mm)	D.D (-)	T (kN.mm)	Failure mode
S1E	1	71	4.21	251.6	43.11	5.84	1.47	8210.96	Flexural failure
S2E	1	94.3	4.38	269.0	35.7	7.54	1.32	7256.70	
S3E	1	110.8	4.73	310.3	23.10	13.43	1.26	5220.76	
S4E	1	117.4	5.32	271.0	35.1	7.72	1.11	7403.07	
S5E	1	120.1	4.99	281.2	34.51	8.15	1.03	7772.96	
S6E	2	157.1	3.08	495.6	11.14	42.11	1.01	7793.34	
S7E	2	152	3.21	462.9	15.29	30.27	1.29	7913.70	
S8E	2	145.6	4.71	435.9	24.84	17.55	1.40	8251.19	

Table 6 The experimental results of group 1 compared to that of the control specimen (S2E)

Specimen model	Group No	P _{cr} /P _{cr} (S2E) %	P _f /P _f (S2E) %	Δ _f /Δ _f (S2E) %	S.S./S.S (S2E) %	D.D/D.D(S2E) %	T/T (S2E) %
S1E	1	75	96	121	77	111	113
S2E	1	100	100	100	100	100	100
S3E	1	117	115	65	178	95	72
S4E	1	124	101	98	102	84	102
S5E	1	127	105	97	108	78	107

Table 7 The experimental results of group 2 compared to that of the control specimen (S6E)

Specimen model	Group No	P _{cr} /P _{cr} (S2E) %	P _f /P _f (S2E) %	Δ _f /Δ _f (S2E) %	S.S./S.S (S2E) %	D.D/D.D(S2E) %	T/T (S2E) %
S6E	1	100	100	100	100	100	100
S7E	1	100	100	100	100	100	100
S8E	1	97	93	137	72	128	102

that beam depth can play a good role in the behavior of hidden and wide beams. Also, it can be very effective in increasing the beam’s ultimate load and decreasing the deflection.

Fig. 11 shows the effect of beam width on the flexural behavior of hidden and wide beams using specimens S2E, S4E, and S5E. The beam width equals 300 mm, 400 mm, and 500 mm for specimens S2E, S4E, and S5E, respectively. The results were compared with the control specimen, S2E, as shown in Table 6. The ultimate load of specimens S4E and S5E showed an insignificant increase of 1% and 5%, respectively, compared to the control specimen S2E. The deflections at ultimate loads of specimens S4E and S5E showed a slight decrease of 2% and 3%, respectively, compared to the control specimen S2E. In general, increasing beam width insignificantly increased the ultimate load while slightly decreasing the deflection of the beams (S4E and S5E) compared to the control specimen S2E.

Fig. 12 shows the effect of beam eccentricity from the column on the flexural behavior of hidden and wide beams, as shown in specimens S6E, S7E, and S8E. The beam eccentricity from the column is taken to be equal to 0, 250 mm, and 350 mm for specimens S6E, S7E, and S8E, respectively. The results were compared with the control specimen (S6E), as shown in Table 7. The ultimate load of specimens S7E and S8E illustrated a decrease of 7% and 12%, respectively, compared to the control specimen S6E. The deflection at the ultimate of specimens S7E and S8E showed an increase of 37% and 123 compared to the control specimen S6E. The results showed that beam-eccentricity from the column must be taken into consideration in the hidden and wide-beam design procedures. The eccentricity of the beam is effective in decreasing the beam’s ultimate load and increasing the deflection at the ultimate load.



Fig. 9 Crack patterns and failure modes for all tested specimens

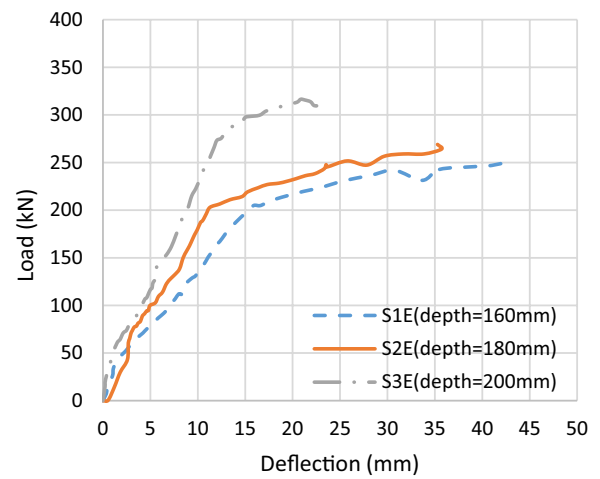


Fig. 10 Load deflection curves of the effect of the beam's depth

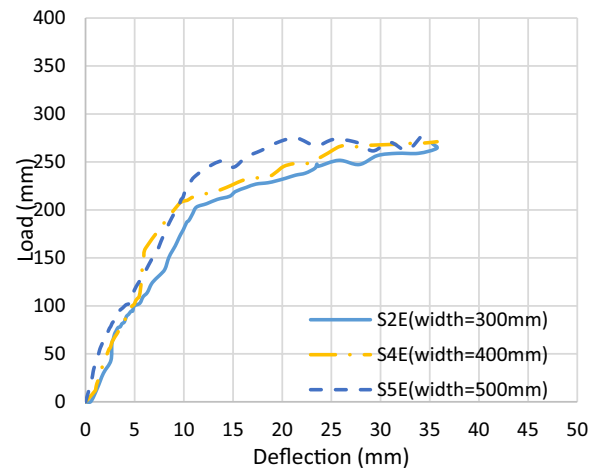


Fig. 11 Load deflection curves of the effect of the beam's width

3.3 Secant Stiffness, Displacement Ductility, and Toughness

Table 6 shows the secant stiffness (S.S.) for the S1E specimen is less than the control specimen S2E, which decreased by 23%, while the S.S. for the S3E specimen is higher than the control specimen S2E, which increased by 78%. The results show that the beam depth has more ductile behavior. Specimens S4E and S5E are slightly higher than the control specimen, which increased by 2% and 8%, respectively. Table 7 shows that the increase in beam width has an insignificant effect on the secant stiffness. The secant stiffness of specimens S7E and S8E is less than that of the control specimen, which decreased by 28% and 58%, respectively. The results show that the decrease in beam eccentricity provides more ductile behavior.

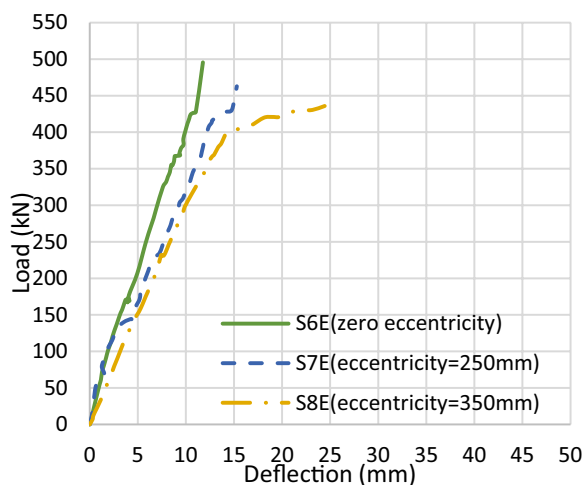


Fig. 12 Load deflection curves of the effect of the beam's eccentricity

As shown in Table 6, the test results show that the displacement ductility (D.D.) for specimens S3E, S4E, and S5E is higher than that of the control specimen by 5%, 7%, 9%, and 23%, respectively. The results show that the displacement ductility (D.D.) improved by decreasing the beam depth and width. As shown in Table 7, the displacement ductility (D.D.) for the S7E and S8E specimens is higher than the control specimen S6E, which increased by 33% and 39%, respectively. The results show that an increase in beam eccentricity leads to more ductile behavior.

Table 6 shows the test results where the toughness (T) for the specimen S1E is higher than the control specimen S2E, which increased by 13%, while the toughness (T) for the specimen S3E is less than the control specimen S2E, which decreased by 28%. The results show that the beam depth improves the toughness. The specimens S4E and S5E are slightly higher than the control specimen S2E, which increased by 2% and 7%, respectively. As shown in Table 7, the toughness (T) for specimens S7E and S8E is higher than the control specimen S6E, which increased by 2% and 6%, respectively. The results show that increasing the beam width and eccentricity increases its toughness.

4 Numerical Analysis

The finite element method has proven to be a reliable tool for determining stresses, internal forces, and deformation in structures during the linear and nonlinear stages of loading. ANSYS V15 (2015) is used to study the load–deflection behavior and failure characteristics of hidden and wide reinforced concrete beams embedded in slabs by analyzing the models and using them to study the

effects of variation in the beam depth, the beam width, and the eccentricity of beams from column support. The analysis showed good agreement between the numerical and experimental results and revealed that hidden and wide beams have behaviors different from projected beams.

4.1 Elements, Loads, and Boundary Conditions

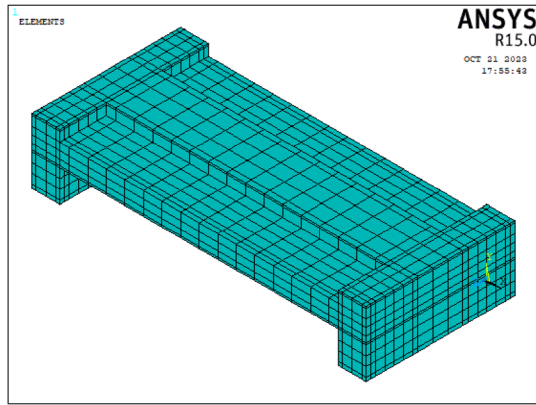
SOLID 65, LINK 180, and SOLID 185 are the most common elements used to represent concrete, reinforcing steel bars, supports, and loading plates under the loads, respectively. SOLID 65 is used for modeling concrete in three dimensions, with or without reinforcing bars (rebar). The element is capable of cracking in tension and crushing in compression. LINK 180 is a 3-D spar element, and it has two nodes with three degrees of freedom per node (translations in x, y, and z directions). SOLID185 is used for the 3-D modeling of steel plates. The element is defined by eight nodes having three degrees of freedom at each node (translations in the nodal x, y, and z directions). Fig. 13 shows the 3-D model for concrete and steel reinforcement.

4.2 Solution Techniques

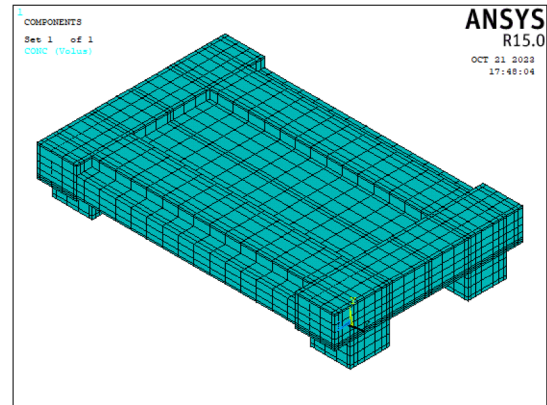
The concrete element has special cracking and crushing capabilities, and its most important aspect is the treatment of nonlinear material properties. The concrete is capable of cracking (in three orthogonal directions), crushing, plastic deformation, and creep. The rebar is capable of tension and compression, but not shear. They are also capable of plastic deformation and creep. The models were solved by using displacement increments until the ultimate failure load.

4.3 Validation Model

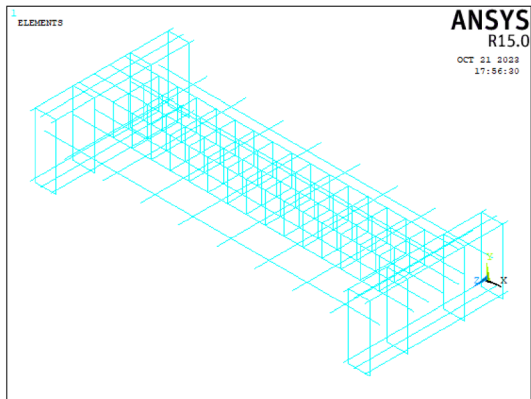
The validation of the numerical model has been conducted by comparing the experimental and numerical results. There is a good agreement between both of them, as shown in Fig. 14. Table 8 compares the numerical and experimental ultimate loads and deflections at the ultimate load. The average and standard deviation show good agreement between measured and predicted load–deflection curves. Fig. 15 illustrates the predicted crack patterns of the numerical models, which can be compared to the observed cracks from the experimental program in Fig. 9. A good agreement has been observed between the predicted and observed cracks from the experimental results. In addition, Table 8 shows the ratio between the predicted ultimate load and deflection at the ultimate load and the measured values from experimental tests. The average of the ratio of the predicted ultimate load and that measured from the experimental work is 1.003 and the standard deviation is 1.981%, and



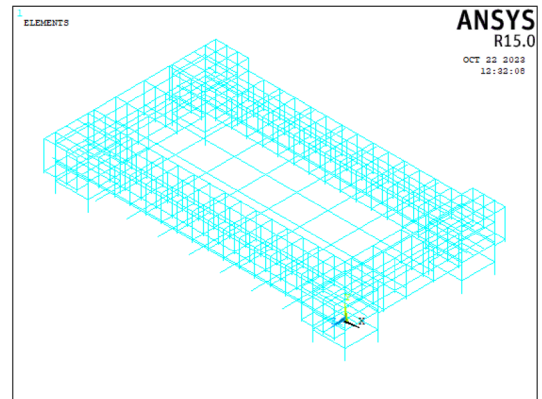
(a) Solid 65 concrete elements (group 1).



(b) Solid 65 concrete elements (group 2).



(c) Link180 reinforced bars (group 1).



(d) Link180 reinforced bars (group 2).

Fig. 13 ANSYS idealization of all tested specimens

these values are 1.03 and 6.004% for deflection at the ultimate load.

5 Parametric Study

The experimental study can't cover the effects of all parameters on the behavior of that kind of beam. Under these circumstances, the numerical study shows an effective and economical alternative. The numerical models were used to extend the experimental studies by employing a suitable numerical model.

5.1 Details of the Studied Beams

The specimens were divided into five groups, as shown in Table 9. Group 1 includes studying the effect of varying concrete characteristics on compressive strength, and Group 2 was used to study the varying steel reinforcement strengths. Group 3 was used to study the bottom reinforcement ratio; Group 4 was used to study the

top-to-bottom reinforcement ratio; and Group 5 was used to study the web reinforcement.

6 Analysis of the Numerical Results

The load–deflection curves illustrate the effect of varying parameters, including ultimate load, deflection, and secant stiffness. Fig. 16 and Table 10 show the effects of the studied parameters on the flexural behavior of hidden and wide beams embedded in slabs.

6.1 Effect of Concrete Compressive Strength

The effect of concrete compressive strength (f_{cu}) was studied using specimens S1P, S2P, and S3P. The concrete compressive strengths (f_{cu}) were equal to 55, 47, and 60 MPa for specimens S1P, S2P, and S3P, respectively. Table 11 and Fig. 16 illustrate that the ultimate load of specimens S1P and S3P is slightly greater than that of specimen S2P by 0.8% and 3.3%, respectively. The

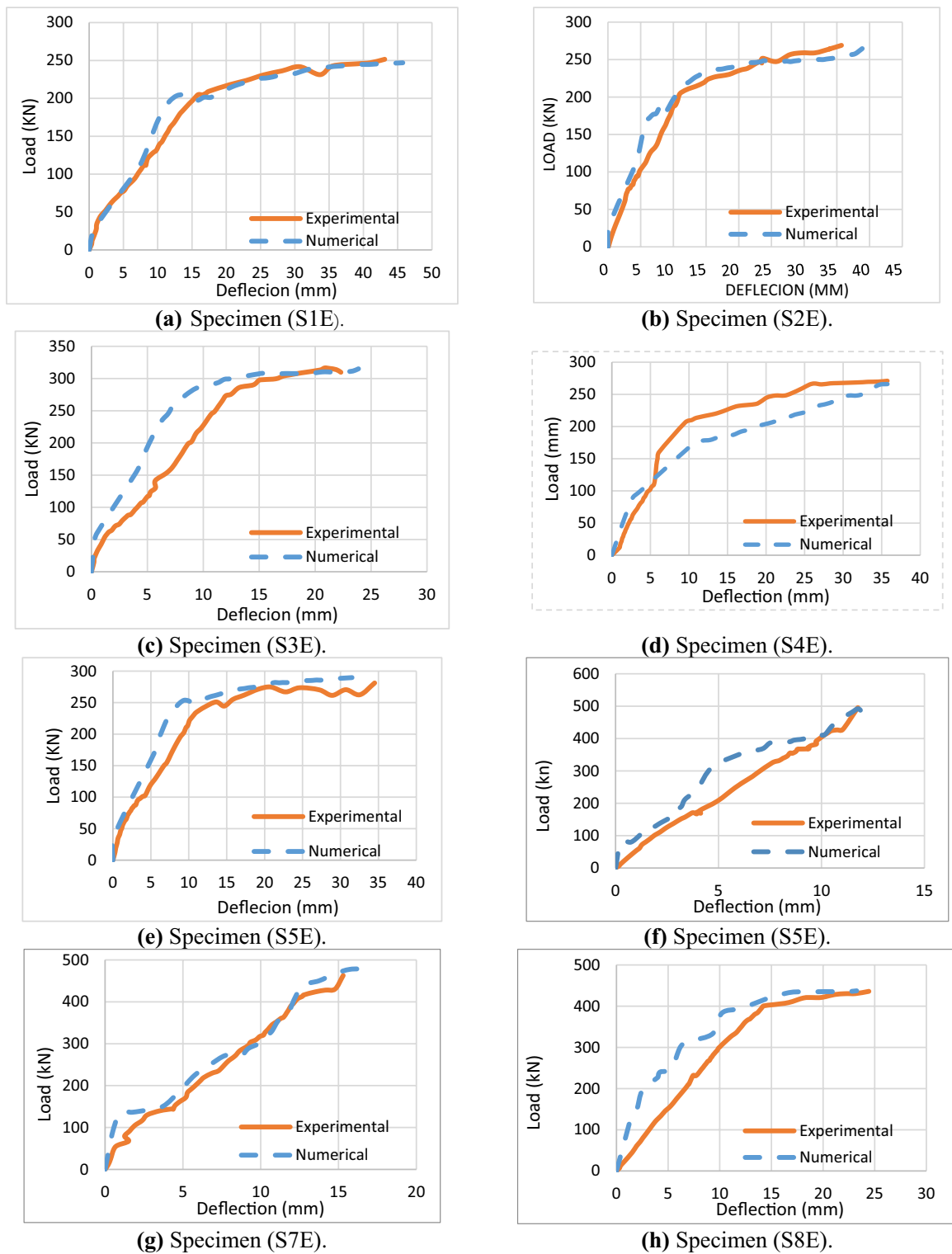


Fig. 14 Experimental and numerical load–deflection curves of all tested specimens

Table 8 Comparison between experimental and numerical results

Specimen model	Group no	Experimental results		Numerical results		Comparison between experimental and numerical results	
		P_f (Exp.) (kN)	Δ_f (Exp.) (mm)	P_u (Num.) (kN)	Δ_u (Num.) (mm)	P_u (Num.)/ P_f (Exp.)	Δ_u (Num.)/ Δ_f (Exp.)
S1E	1	251.6	43.11	246.98	45.75	0.982	1.061
S2E	1	269.0	35.7	264.63	38.875	0.984	1.089
S3E	1	310.3	23.10	315.102	23.875	1.015	1.034
S4E	1	271.0	35.10	266.011	35.75	0.982	1.019
S5E	1	281.2	34.51	289.71	31.524	1.030	0.913
S6E	2	495.6	11.14	492.04	11.97	0.993	1.075
S7E	2	462.9	15.29	477.95	16.75	1.033	1.095
S8E	2	435.9	24.43	437.21	23.25	1.003	0.936
Average						1.003	1.030
Standard deviation						0.020	0.062
Standard deviation (%)						1.981	6.004

deflections at the ultimate load of specimens S1P and S3P are less than those of S2 by 19.3% and 23.2%, respectively. In addition, the secant stiffness of specimens S1P and S3P is greater than that of specimen S2P by 15% and 25.4%, respectively. Hence, the greater the ultimate compressive strength, the greater the ultimate load, and the greater the secant stiffness, the less the deflection at the ultimate load. With the increase in the concrete compressive strength, the ultimate load and the secant stiffness increased, along with a decrease in the deflection.

6.2 Effect of Steel Reinforcement Strength

Two specimens are analyzed using ANSYS V15 (ANSYS V15, 2015) to study the effect of reinforcement yield strength. The reinforcement yield strength was 400 and 360 MPa for specimens S4P and S5P, respectively, compared to the control slab S2P, which had a yield strength of 500 MPa. Table 12 and Fig. 16 illustrate that the ultimate load of specimens S4P and S5P is less than the control specimen S2P by 8.9% and 14.3%, respectively. The deflections at the ultimate load of beams S4P and S5P are greater than those of S2P by 12.8% and 6.7%, respectively. In addition, the secant stiffness of specimens S4P and S5P is less than that of specimen S2P by 28.6% and 38%, respectively. A decrease in the reinforcement yield strength results in a decrease in the ultimate load and secant stiffness and an increase in the deflection.

6.3 Effect of the Bottom Reinforcement Ratio

To study the effect of the bottom reinforcement ratio on deflection at the ultimate load, secant stiffness, and ultimate load, the results of the two specimens, S6P and S7P,

are compared to the control specimen, S2P, as shown in Table 12. Table 12 and Fig. 16 illustrate that the ultimate load of specimen S6P is less than the control specimen S2P by 2.8%. The ultimate load of specimen S7P is greater than that of specimen S2P by 72.1%. The deflection at the ultimate load of specimen S6P is greater than that of S2P by 3.5%. The deflection at the ultimate load of specimen S7P is less than that of S2P by 61.7%. In addition, the secant stiffness of specimen S6P is less than that of specimen S2P by 48.7%, while the secant stiffness of specimen S7P is greater than that of specimen S2P by 239.2%. The decrease in the bottom reinforcement ratio leads to a decrease in the ultimate load and secant stiffness while increasing deflection. A decrease in the reinforcement yield strength results in a decrease in the ultimate load and secant stiffness and an increase in deflection.

6.4 Effect of the Top-to-Bottom Reinforcement Ratio

Two specimens, S8P and S9P, compared to the control specimen, S2P, are shown in Table 12 and Fig. 16 study the effect of the bottom-to-top reinforcement ratio on a deflection at ultimate load, ultimate load, and secant stiffness. The ultimate load of specimens S8P and S9P is slightly less than that of specimen S2P by 2.6% and 0.4%, respectively, while the deflections at the ultimate load of beams S8P and S9P are greater than that of S2P by 5.1% and 2.6%, respectively. In addition, the secant stiffness of specimens S8 and S9P is less than that of specimen S2P by 29.4% and 24.5%, respectively. It is clear from the decrease in the top-to-bottom reinforcement ratio, the decrease in the ultimate load, the secant stiffness, and the increase in the deflection.

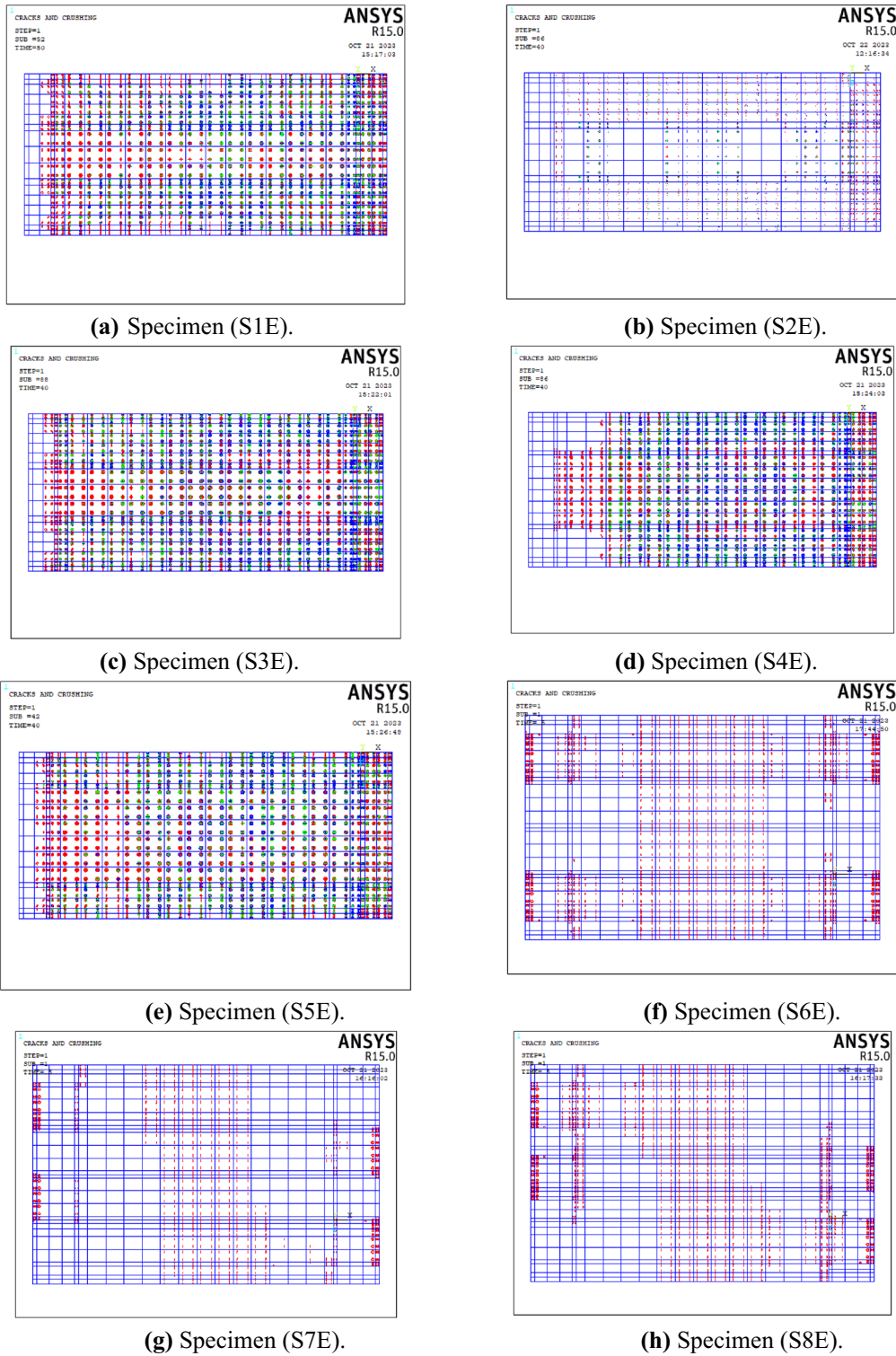


Fig. 15 Numerical predicted crack patterns and failure modes of all tested specimens

Table 9 Details of the specimens used in the parametric study

Specimen model	Group no	Studied parameters					Notes
		f_{cu} (MPa)	f_y (MPa)	Bottom RFT ratio	A_s top/ A_s bottom	Web RFT	
S1P	1	55	500	0.2 μ max	1	10 Φ 8/m–4 branches	Effect of concrete strength f_{cu}
S2P (Control)		47	500	0.2 μ max	1	10 Φ 8/m–4 branches	
S3P		60	500	0.2 μ max	1	10 Φ 8/m–4 branches	
S4P	2	47	400	0.2 μ max	1	10 Φ 8/m–4 branches	Effect of reinforcement strength f_y
S2P		47	500	0.2 μ max	1	10 Φ 8/m–4 branches	
S5P		47	360	0.2 μ max	1	10 Φ 8/m–4 branches	
S6P	3	47	500	μ min	1	10 Φ 8/m–4 branches	Effect of the bottom reinforcement ratio
S2P		47	500	0.2 μ max	1	10 Φ 8/m–4 branches	
S7P		47	500	μ max	1	10 Φ 8/m–4 branches	
S8P	4	47	500	0.2 μ max	0.4	10 Φ 8/m–4 branches	Effect of A_s Top/ A_s Bottom
S2P		47	500	0.2 μ max	0.6	10 Φ 8/m–4 branches	
S9P		47	500	0.2 μ max	1	10 Φ 8/m–4 branches	
S10P	5	47	500	0.2 μ max	1	10 Φ 8/m–4 branches	Effect of web reinforcement
S2P		47	500	0.2 μ max	1	10 Φ 10/m–4 branches	
S11P		47	500	0.2 μ max	1	10 Φ 12/m–4 branches	

Where RFT is the reinforcement, (t_b/L) is the ratio of beam width to the span 1/10; (b_b/b_c) is the beam width to column width = 1.0; and (e/b_c) is the ratio of beam eccentricity to column width = 0.0

6.5 Effect of Web Reinforcement

The two specimens, S10P and S11P, were used to study the effect of the web reinforcement on the deflection at the ultimate load and secant stiffness. The results were compared to the control specimen, S2. Table 12 and Fig. 16 illustrate that the ultimate load of specimens S10P and S11P is greater than that of specimen S2P by 1.5% and 2.1%, respectively. The deflections at the ultimate load of beams S10P and S11P are less than that of S2 by 15.4% and 23.2%, respectively. In addition, the secant stiffness of specimens S10P and S11P is greater than that of specimen S2P by 14% and 22.6%, respectively. Hence, the greater the web reinforcement, the greater the ultimate load and the secondary stiffness, while the less the deflection at the ultimate load. The increase in the web reinforcement increases the ultimate load and the secondary stiffness while decreasing the deflection.

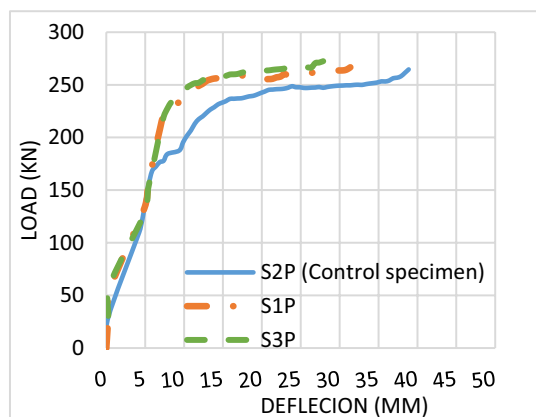
7 Analytical Models

Table 11 illustrates the comparison between the experimental and analytical results calculated from the ECP 203-2019 code (ECP-203, 2019) and the ACI 318-19 code (ACI Committee 319-19, 2019). The average ratio of the experimental ultimate load and that calculated from the ECP 203-2019 code (ECP-203, 2019) and the ACI 318-19 (ACI Committee 319-19, 2019) is 94.4% and 92%, respectively. The standard deviation for the ECP 203-2019 code (ECP-203, 2019) and ACI 318-19 (ACI Committee 319-19, 2019) is 5.23% and 4.43%, respectively. Table 12

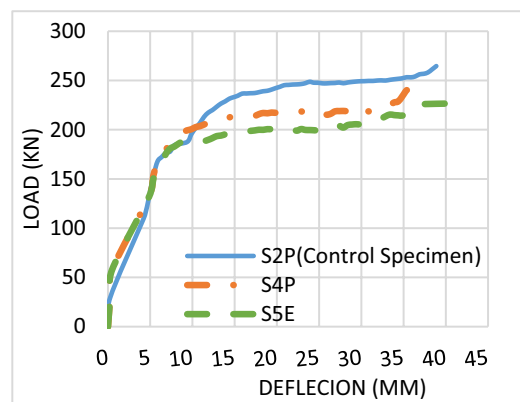
illustrates the comparison between the numerical and analytical results calculated from the ECP 203-2019 code (ECP-203, 2019) and the ACI 318-19 code (ACI Committee 319-19, 2019). The average ratio of the experimental ultimate load and that calculated from the ECP 203-2019 code (ECP-203, 2019) and the ACI 318-19 (ACI Committee 319-19, 2019) is 90.1% and 88.2%, respectively. The standard deviation for the ECP 203-2019 code (ECP-203, 2019) and the ACI 318-19 (ACI Committee 319-19, 2019) is 5.97% and 5.91%, respectively. The comparison showed agreement between the experimental and numerical results and those calculated from the ECP 203-2019 code (ECP-203, 2019) and the ACI 318-19 code (ACI Committee 319-19, 2019).

8 Conclusion

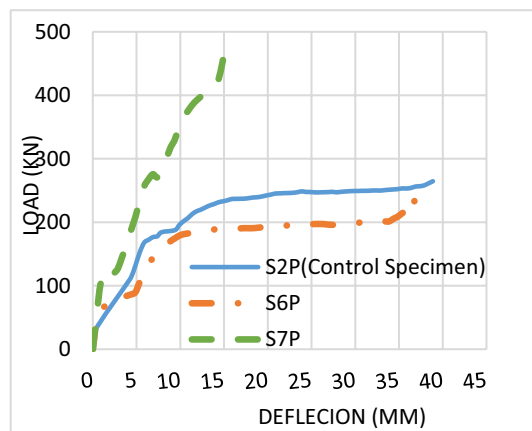
This paper introduces an experimental study of eight specimens to investigate the flexural behavior of hidden and wide beams embedded in slabs. The three studied parameters are (1) the beam depth, (2) the beam width, and (3) the beam eccentricity from the column support. In addition, nonlinear finite element analysis using the ANSYS V.15 program has been implemented. The numerical modeling of the tested specimens and other full-scale specimens was investigated through a parametric study. The numerical models were used to validate the experimental results. Also, the numerical models discuss other parameters. The studied parameters were (1) concrete compressive strength (f_{cu}); (2) steel reinforcement



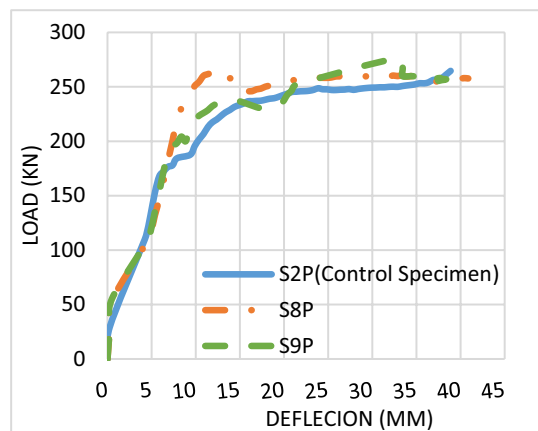
(a) Group 1: Effect of concrete strength (f_{cu})



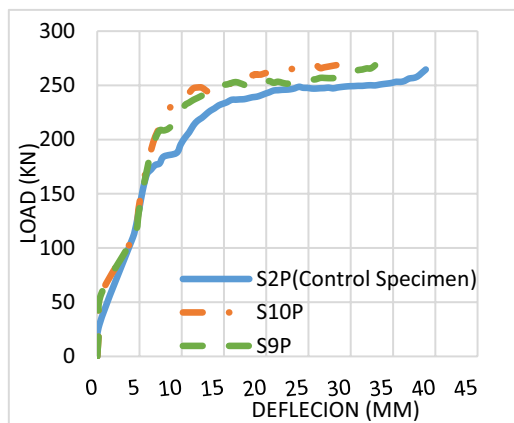
(b) Group 2: Effect of reinforcement strength (f_y)



(c) Group 3: Effect of bottom reinforcement ratio



(d) Group 4: Effect of $A_{s Top}/A_{s Bottom}$.



(e) Group 5: Effect of Web Reinforcement.

Fig. 16 Load–deflection curves of all studied specimens

Table 10 Numerical results

Specimen model	P_u (Num) (kN)	Δ_u (Num) (mm)	Secant stiffness (S.S) (kN/mm)	P_u/P_{uS2P} %	Δ_u/Δ_{uS2P} %	S.S./S.S.S2P %
S1E	266.65	31.38	8.499	1.008	0.807	1.150
S2E	264.63	38.88	6.807	1.000	1.000	1.000
S3E	273.32	29.88	9.149	1.033	0.768	1.254
S4E	241.11	43.88	5.495	0.911	1.128	0.714
S5E	226.55	41.50	5.464	0.857	1.067	0.620
S6E	257.26	37.52	6.857	0.972	0.965	0.513
S7E	455.50	14.88	30.612	1.721	0.383	3.392
S8E	257.69	40.88	6.304	0.974	1.051	0.706
S9E	263.62	39.88	6.611	0.996	1.026	0.755
S10E	268.52	32.88	8.168	1.015	0.846	1.140
S11E	270.22	29.88	9.045	1.021	0.768	1.226

yield strength (f_y); (3) the bottom reinforcement ratio (μ/μ_{max}); (4) the top-to-bottom reinforcement ratio ($A_{s\ top}/A_{s\ bottom}$); and (5) web reinforcement. Finally, the experimental and numerical results were compared with those calculated based on the ECP 203-19 code (ECP-203, 2019) and the ACI 318-19 code (ACI Committee 318-19, 2019). The comparison was satisfactory. Based on the experimental, numerical, and analytical results and the range of the studied parameters, the following are the main conclusions:

1. The beam depth is an effective parameter in the behavior of hidden and wide beams. By decreasing the beam depth, ductile behavior can be obtained. An increase in beam ductility of 11% was predicted due to a decrease in beam depth of 11%. A decrease in beam depth enhances its toughness by 13% when the beam depth is decreased by 11%. The beam depth effectively increases the hidden and wide beam's ultimate load by 15% due to increasing the beam depth by 11% and decreasing deflection by 35%.
2. The beam width insignificantly increases the hidden and wide beam's ultimate load, where the increase is 1% due to an increase in the beam width of 33%. The beam width slightly decreases the deflection, where the decrease is 2% due to increasing the beam width by 33%. A decreasing beam width of 33% improves displacement ductility by 16%.
3. The beam eccentricity from the column must be taken into consideration in the hidden and wide beam design procedure, and the designers must consider the eccentricity. The beam eccentricity from its support plays a significant role in decreasing the hidden and wide beam's ultimate load by 7% due to an increase in the eccentricity of 100% and increasing the deflection by 37%. By decreasing the beam eccentricity, more ductile behavior can be achieved. The displacement-ductility increased by 28% due to the increase in beam eccentricity by 100%. By increasing eccentricity by 100%, an insignificant improvement of 2% in toughness was achieved.
4. The grade of the concrete plays a significant role in the behavior of hidden and wide beams. The greater the concrete compressive strength, the greater the ultimate load and secant stiffness, while the smallest the deflection. Increasing the concrete compressive strength by 28% increases the ultimate load and secant stiffness by 3% and 25%, respectively, and decreases the deflection by 23%.
5. Decreasing reinforcement yield strength, decreasing the ultimate load and secant stiffness, and increasing deflection, where a decrease of 28% in the reinforcement yield strength decreases the ultimate load and secant stiffness by 14% and 38%, respectively, while increasing the deflection by 7%.
6. The increase in the flexural reinforcement ratio by 100%, the increase in the ultimate load and the secant stiffness by 72% and 239%, respectively, and a decrease in the deflection by 62%.
7. Decreasing the top-to-bottom reinforcement ratio by 60%, decreasing the ultimate load and secant stiffness by 3% and 29%, respectively, and increasing the deflection by 5%.
8. The effectiveness of beam web reinforcement decreases as the spacing of the web reinforcement legs across the width of the wide beams increases. The shear strength provided by stirrups remains overvalued when transversal reinforcement (stirrups with very few legs.) is used. By increasing the beam-web reinforcement ratio by 56%, the ultimate

Table 11 Comparison of the experimental and analytical results

Specimen model	Group No	Experimental results P_{uExp} (kN)	Analytical results		Comparison between experimental and analytical results		
			P_{uACI} (kN)	P_{uECP} (kN)	P_{uECP}/P_{uExp} %	P_{uACI}/P_{uExp} %	P_{uACI}/P_{uECP} %
S1E	1	251	220.26	218.77	0.87	0.88	1.011
S2E	1	269.0	244.32	250.72	0.93	0.91	0.978
S3E	1	310.3	276.27	282.68	0.91	0.89	0.978
S4E	1	271.0	245.07	250.76	0.93	0.90	0.968
S5E	1	281.2	247.19	251.33	0.89	0.88	0.989
S6E	2	495.6	432.39	449.84	0.91	0.87	0.956
S7E	2	462.9	432.39	449.84	0.97	0.93	0.959
S8E	2	435.9	432.39	449.84	1.03	0.99	0.961
Average					0.93	0.91	0.98
Standard deviation					0.047	0.036	0.017
Standard deviation (%)					5.043	4.014	1.780

Table 12 Comparison of the numerical and analytical results

Specimen model	Group No	Experimental results P_{uExp} (kN)	Analytical results		Comparison between experimental and analytical results		
			P_{uACI} (kN)	P_{uECP} (kN)	P_{uECP}/P_{uExp} %	P_{uACI}/P_{uExp} %	P_{uACI}/P_{uECP} %
S1E	1	266.65	244.29	250.61	0.92	0.94	0.981
S2E	1	264.63	244.31	250.72	0.92	0.95	0.976
S3E	1	273.32	244.77	250.69	0.90	0.92	0.984
S4E	1	241.11	198.64	201.64	0.82	0.84	0.986
S5E	1	226.55	180.11	181.96	0.80	0.80	0.991
S6E	2	257.26	210.19	214.54	0.82	0.83	0.981
S7E	2	455.50	372.36	392.87	0.82	0.86	0.950
S8E	2	257.69	244.31	248.78	0.95	0.97	0.983
S9E	2	263.62	244.31	249.75	0.93	0.95	0.979
S10E	2	268.52	244.31	250.72	0.91	0.93	0.976
S11E	2	270.22	244.31	250.72	0.89	0.93	0.957
Average					0.88	0.90	0.977
Standard deviation					0.052	0.054	0.012
Standard deviation (%)					5.909	5.974	1.017

load and the secant stiffness were increased by 1.5% and 14%, respectively, while increasing the beam-web reinforcement ratio, the deflection decreased by 15%.

9. The results of the numerical and analytical study show adequate agreement with the results of the experimental investigation. The mean and standard deviation show good agreement between the experimental and numerical results and those calculated from the ECP 203-2017 and the ACI 318-19 codes. The ultimate loads calculated from ECP 203-2019 and the ACI 318-19 codes are conservative compared to the experimental ones. The mean and the standard

deviation for both codes are 93%, 5%, 91%, and 4%, respectively, compared to the experimental results. The mean and the standard deviation of the ultimate loads calculated from the ECP 203-2019 and the ACI 318-19 codes are 90%, 5.97%, 88%, and 5.9%, respectively, compared to the numerical results. The ultimate load calculated according to the ECP 203-2019 code is more accurate than the ACI 318-19 code for the range of the studied parameters. Both ECP 203-2019 and ACI 318-19 code provisions should be revised to take into consideration the effects of beam

width, beam eccentricity, web reinforcement, and top and bottom steel reinforcement ratios.

List of symbols

Δ_{cr}	Deflection at the first crack load
Δ_u	Deflection at the ultimate failure load
P_{cr}	First crack load
P_f	Failure load
$P_{cr (exp)}$	Experimental first crack load
$P_{f (exp)}$	Experimental failure load
$P_{u (ana)}$	Analytical ultimate failure load
$\Delta_{cr (Num)}$	Numerical first crack load
$\Delta_u (Num)$	Numerical ultimate failure load
f_{cu}	Average concrete cubic compressive strength
f_c	Average cylindrical compressive strength of concrete
f_y	Main steel reinforcement yield strength
RFT	Steel reinforcement.
D.D.	Displacement ductility, which is the ratio of the displacement at 90% of the failure load in the descending branch to that in the ascending branch
S.S.	Secant stiffness (P_u/Δ_u)
T	Toughness, which equals the area under the load–deflection curve

Acknowledgements

The authors carried out the experimental work in the laboratory of the Faculty of Engineering at Mataria, Helwan University, Egypt. The authors acknowledged the help and assistance offered by the laboratory staff.

Author contributions

Ahmed A. Mahmoud, corresponding author: He actively participated in the research plan and assisted in how to implement the practical and theoretical program and review the paper. Conceptualization, methodology, project administration, validation, supervision, writing, reviewing, and editing the paper. Belal K. El Gani: He implemented the experimental and analytical programs. Data curation includes formal analysis, funding acquisition, investigation, and writing the original draft. Tarek S. Mostafa: Carried out a technical and linguistic review of the paper before submitting it, methodology, software, supervision, and writing the original draft. Ahmed N. Khater: Check the paper carefully, review it, and try to make it in the final form. Resources, software supervision, and writing the original draft. All the authors declare their contributions to the paper preparation (experimental, numerical, and analytical activities, discussions, and paper reading and writing).

Funding

Open access funding provided by The Science, Technology & Innovation Funding Authority (STDF) in cooperation with The Egyptian Knowledge Bank (EKB). The authors didn't receive any specific grants from funding agencies in the public, commercial, or not-for-profit sectors. This research received no external funding.

Availability of data and materials

The authors include all data generated or analyzed during the study in this published article and its supplementary information files. The datasets used and analyzed during the current study are available from the corresponding author upon reasonable request.

Declarations

Ethics approval and consent to participate

The authors declare their ethical approval and consent to participate.

Consent for publication

The authors declare consent for publication.

Competing interests

The authors declare that they have no competing interests. The authors declare that they have no known competing financial interests or personal

relationships that could have appeared to influence the work reported in this paper.

Received: 17 February 2024 Accepted: 26 June 2024

Published online: 22 October 2024

References

- Abbas, A. L., & Hassan, Y. R. (2019). Shear behavior of reinforced concrete wide beams strengthened with CFRP sheet without stirrups. *DJES Diyala Journal of Engineering Sciences*. <https://doi.org/10.24237/djes.2019.12110>
- ACI Committee 318-19. (2019). *Building code required for reinforced concrete (ACI 318-19) and commentary (ACI 318R-19)*. American Concrete Institute. <https://doi.org/10.14359/51716937>
- Alluqmani, A. E. (2020). Effect of the transversal spacing of stirrup legs on the behavior and strength of shallow concealed RC beams. *Journal of Engineering Design and Technology*. <https://doi.org/10.1108/JEDT-06-2020-0224/full/html>
- Al-Negheimish, A. I., El-Sayed, A. K., Al-Zaid, R. A., Shuraim, A. B., & Alhozaimey, A. M. (2011). The behavior of wide, shallow RC beams strengthened with CFRP reinforcement. *Journal of Composites for Construction*. [https://doi.org/10.1061/\(ASCE\)CC.1943-5614.0000274](https://doi.org/10.1061/(ASCE)CC.1943-5614.0000274)
- ANSYS V15. (2015). *Manual set*. ANSYS Inc. <https://www.ansys.com/academic/learning-resources8ihx.pdf>
- ASTM E8/ASTM E8m. (2013). *Standard test method for tensile testing of metallic materials*. <https://www.zwickroell.com/industries/metals/metals-standards/metals-tensile-test-astm-e8/>. DOI: 10.1520/E0008_E0008M-13A.
- ASTM International. (2015a). *Standard test method for compressive strength of cylindrical concrete specimens*. ASTM C39/C39M-14. https://doi.org/10.1520/C0039_C0039M-14. <https://www.studocu.com/row/document/state-engineering-university-of-armenia/concrete-design/astm-c39-c39m-14-concrete-design/32367366>.
- ASTM International. (2015b). *Standard test method for splitting the tensile strength of cylinder concrete specimens*. ASTM C496-96. <https://doi.org/10.1520/C0496-96>. <https://www.astm.org/c0496-96.html>
- ASTM International. (2014). *Standard test method for static modulus of elasticity and Poisson ratio of concrete in compression*. ASTM C469/C469M-14, West Conshohocken. https://doi.org/10.1520/C0469_C0469M-14. https://www.astm.org/c0469_c0469m-14.html.
- Behnam, H. A. (2018). Parametric finite element analysis of RC wide beam-column connections. *Computers & Structures*, 205(1), 28–44. <https://doi.org/10.1016/j.compstruc.2018.04.004>
- Conforti, A., Minelli, F., & Plizzari, G. A. (2013). Wide-shallow beams with and without steel fibers: a peculiar behavior in shear and flexure. *Composites Part B Engineering*, 51, 282–290. <https://doi.org/10.1016/j.compositesb.2013.03.033>
- Conforti, A., Minelli, F., Tinini, A., & Plizzari, G. A. (2015). Influence of polypropylene fiber reinforcement and width-to-effective depth ratio in wide-shallow beams. *Engineering Structures*, 88, 12–21. <https://doi.org/10.1016/j.engstruct.2015.01.037>
- ECP-203. (2019) *Egyptian code of practice for design and construction of reinforced concrete structures* (pp. 39–41) Housing and Building Research Center, Ministry of Building and Construction. <https://www.scribd.com/document/392618589/ECP-203-2017-pdf>
- El Bannani, A. S. (2013). *Shear behavior of reinforced concrete wide beams*. MSc. Thesis, Department of Civil Engineering, Cairo University, Cairo, Egypt. <https://eng.cu.edu.eg/en/m-sc-and-ph-d-thesis/>.
- Helou, S. H., & Awad, R. (2014) Performance-based analysis of hidden beams in reinforced concrete structures. In: *Conference: Nonlinear Structural Dynamics, at Aghadir-Morocco*. <https://doi.org/10.1051/mateconf/2014610001>. <http://www.mateconferences.org>. https://www.researchgate.net/publication/266022357_Performance_based_analysis_of_hidden_beams_in_reinforced_concrete_structures
- Helou, D. H., & Diab, M. (2014). Slabs with concealed beams: facts and fallacies. *Asian Journal of Engineering and Technology*, 2(4), 2321–2462.
- Ibrahim, A. M., Mansor, A. A., Salman, W. D., & Hamood, M. J. (2018). Strength and ductility of bubbled wide reinforced concrete beams with diverse types of shear steel plates. *International Journal of Engineering and Technology*, 7(4), 502–506. <https://doi.org/10.14419/ijet.v7i4.20.26251>

- Khalil, A. H. (2019). The effective width in the shear design of wide-shallow beams: A comparative study. *Journal of Civil Engineering*, 23, 1670–1681. <https://doi.org/10.1007/s12205-019-0830-7>
- Lotfy, E. M., Mohamadien, H. A., & Hassan, H. M. (2014). Effect of web reinforcement on shear strength of shallow, wide beams. *International Journal of Engineering and Technical Research (IJETR)*, 2(11), 98–107.
- Mawlood, B., Mohammad, A. H., Ismail, K. S., & Abdulrazzaq, N. M. (2021). Shear strength of reinforced high-performance concrete wide beams. *ZANCO Journal of Pure and Applied Sciences*, 33(2), 117–127. <https://doi.org/10.21271/ZJPAS.33.2.11>
- Moawad, M. S. (2021). Effect of short glass fiber on the shear capacity for shallow wide reinforced concrete beams. *Journal of Engineering and Applied Science*, 46, 4747–4763.
- Mohammed, A. S., Al-Zuheriy, A. S. J., & Abdulkareem, B. F. (2023). An experimental study to predict a new formula for calculating the deflection in wide concrete beams reinforced with shear steel plates. *International Journal of Engineering*. <https://doi.org/10.5829/IJE.2023.36.02B.15>
- Morsy, N. S., Alaa, G., Shoeib, S. A. E., & Agamy, M. H. (2018). Experimental study of enhancing the shear strength of hidden and shallow beams by using shear reinforcement. In: *Proceeding of the 3rd World Congress on Civil, Structural, and Environmental Engineering (CSEE'18)*. (Vol. 18). <https://doi.org/10.11159/icsenm18.116>.
- Nadagouda, M. I., & Ravi, G. (2017). Analytical study on the flexural behavior of RCC slabs with concealed beams using ANSYS. *International Research Journal of Engineering and Technology (IRJET)*, 4(7), 3094–3101.
- Olvera, C. Z., Burneo, D. V., Troncoso, N. G., Silva, C. E., Gómez, P. D., & Bompá, D.V. (2023). Comparative analysis of the seismic behavior of low-rise buildings with hidden and drop beams. In: *21st LACCEI International Multi-Conference for Engineering, Education, and Technology* (pp. 1–9). https://laccei.org/LACCEI2023-BuenosAires/papers/Contribution_219_a.pdf. ISBN: 978-628-95207-4-3. ISSN: 2414-6390. Digital Object Identifier: <https://doi.org/10.18687/LACCEI2023.1.1.219>
- Ozbek, E., Aykac, B., & Bocek, M. (2019). The behavior and strength of hidden RC beams embedded in slabs. *Journal of Building Engineering*, 29(2), 101130. <https://doi.org/10.1016/j.jobbe.2019.101130>
- Talawar, C., & Sonawadekar, N. (2017). Performance-based analysis of concealed beams in reinforced concrete structures. *International Research Journal of Engineering and Technology (IRJET)*, 4(6), 5.
- Tapan, M. (2014). Structural response of reinforced concrete wide beams reinforced with lattice girders. *Iranian Journal of Science and Technology Transactions of Civil Engineering*, 38(2), 337–344.
- Yasouj, M., Marsono, A. K., Abdullah, R., & Moghadasi, M. (2015). Wide beam shear behavior with diverse types of reinforcement. *ACI Structural Journal*, 112(2), 199–208. <https://doi.org/10.14359/51687299>
- Yousef, A. M., Marami, N. A., & Tahwia, A. M. (2023). Experimental and numerical investigation for torsional behavior of UHPFRC shallow and deep beams. *Arabian Journal for Science and Engineering*. <https://doi.org/10.1007/s13369-023-07701-3>

Publisher's Note

Springer Nature remains neutral with regard to jurisdictional claims in published maps and institutional affiliations.

Ahmed A. Mahmoud Professor of R.C. Structures, Civil Engineering Department, Faculty of Engineering (Shoubra), Benha University, Cairo, Egypt.

Belal K. El Gani Research Assistant, Civil Engineering Department, Faculty of Engineering (Shoubra), Benha University, Cairo, Egypt.

Tarek S. Mustafa Associate Professor, Civil Engineering Department, Faculty of Engineering (Shoubra), Benha University, Cairo, Egypt.

Ahmed N. M. Khater Assistance Professor, Civil Engineering Department, 0000-0003- ahmed.khater@feng.bu.edu.eg Faculty of Engineering (Shoubra), Benha University, Cairo, Egypt.